Analysis and modelling of flame speed in autoigntive mixtures of n-heptane and methane

Bruno S. Soriano[a,*], Edward S. Richardson[a]

[a] *Faculty of Engineering and the Environment, University of Southampton, Southampton, UK*

Abstract

The effects of pre-ignition chemistry on laminar flame speed in methane/n-heptane fuel blends are investigated numerically, leading to flame speed modelling accounting for these effects. The laminar flame speeds of fuel blends are important input parameters for turbulent combustion models needed to support design of dual-fuel engines. At the autoignitive conditions found in engines, pre-ignition reactions cause the speed of the reaction front to increase. Fuels that exhibit two-stage ignition behaviour, such as n-heptane, also exhibit a two-stage increase in the speed of the reaction front as the reactant residence time increases. There is a corresponding reduction in the flame thickness until the residence time approaches the ignition delay time, whereupon the deflagrative scaling of flame thickness breaks down. The analysis shows that the increase in flame speed is due to distinct contributions of heat release, reactant consumption, and enhanced reactivity ahead of the flame. Addition of methane to n-heptane–air mixtures retards and reduces the first-stage increase in flame speed, in part due to dilution of the more-reactive n-heptane fuel, and in part due to consumption of radical species by the methane chemistry. The effect of methane/n-heptane fuel blending on flame speed is described adequately by a linear mixing rule. The effect of pre-ignition chemistry can then be modelled as a linear function of the progress variable ahead of the flame – accounting for heat release, reactant consumption, and enhanced reactivity ahead of the flame.

*Corresponding author
Email address: b.s.soriano@soton.ac.uk (Bruno S. Soriano)

The flame speed model accurately describes the variation of flame speed across the full range of methane/n-heptane blends at engine-relevant conditions, up to the deflagaration/ignition transition.

Keywords: cool-flame, low temperature chemistry, two-stage ignition, residence time, flame speed, dual-fuel

---

1. Introduction

High efficiency engines require high temperature and high pressure combustion conditions – conditions at which the reactants may become autoignitive. Even in engine systems nominally characterised by deflagarative combustion, flame propagation may still be affected by the pre-ignition chemical reactions taking place ahead of the flame. Such reactions can affect flame stability and prompt flashback in steady-flow combustors [1], and affect ignitability [2], heat release rates [3] and detonation phenomena [4] in piston engines. Ignition chemistry differs markedly among fuels, with heavier hydrocarbon fuels exhibiting two-stage ignition under some conditions [5], leading to differences in the structure and speed of flame propagation through autoignitive mixtures [6]. These differences may be particularly relevant in dual fuel engines in which fuels with dissimilar ignition behaviours, such as natural gas and diesel, are introduced separately [7]. However the effect that blending fuels with dissimilar ignition chemistry has on flame propagation through autoignitive mixtures is not well characterised.

Hydrogen and light hydrocarbon fuels such as methane exhibit single-stage high-temperature ignition behaviour. Pre-ignition reactions have limited effect on flame propagation through single-stage ignition mixtures until the mixture is close to the point of autoignition [6, 8]. In contrast, heavier hydrocarbons relevant to real transport fuels, such as n-heptane, exhibit low temperature chemistry (LTC) [9] and *cool flames* [10]. The chemical kinetics controlling cool flames arise at high pressure and moderate temperatures, and are closely related to those of two-stage ignition and Negative Temperature Coefficient

(NTC) behaviour [5, 11]. Low temperature chemistry can significantly modify the chemical and transport properties of a mixture [3], thereby affecting the laminar flame speed well before the occurrence of high-temperature ignition [6, 12]. The response of laminar flame properties to blending of fuels with dissimilar ignition behaviours, such as methane and n-heptane, has not been characterised fully at autoignitive conditions. Methane/n-heptane mixtures are of particular interest because these have been used in research studies as surrogate fuels for the natural gas/diesel mixtures arising in pilot-ignited dual fuel engines [e.g. 13, 14, 15].

The laminar flame speed and laminar flame thickness are centrally important in characterisation and modelling of turbulent combustion in engines because they directly affect the turbulent flame speed [16]. The dependence of the turbulent flame speed on laminar flame properties persists for flames affected by LTC [1, 3]. Knowledge of the laminar flame speed and laminar flame thickness are therefore key to understanding and modelling combustion processes under the autoignitive conditions that predominate in practical combustion systems. However established empirical models for the variation of flame speeds with temperature, pressure, equivalence ratio and dilution, such as in Ref. [17], do not account for the effect of pre-ignition chemical processes on flame speed.

Laminar flame speed. Pre-ignition chemical reactions ahead of a flame affect the propagation speed. As such, there is not a unique freely-propagating laminar flame speed (s_l) at autoignitive conditions. Rather, the flame speed depends on the extent of the pre-ignition reactions ahead of the flame [6, 8, 12], which can be related to the residence time τ_f of the reactants upstream of the flame front [18]. A non-autoignitive freely-propagating laminar flame corresponds to the limit where the residence time is much less than the ignition delay time, $\tau_f \ll \tau_{ign}$, whereas the limit $\tau_f \rightarrow \tau_{ign}$ corresponds to the transition from a deflagarative flame to a pure ignition front [19].

The propagation speed of the flame front can be evaluated in a general way from the density-corrected displacement speed s_f, given by $s_f = \rho s_d / \rho_u$, where

ρ and s_d are the local density and displacement speed, and ρ_u is the density of the unburnt reactants [20]. Evaluating s_f in any unstrained one-dimensional stationary flame configuration yields a well-defined residence time-dependent flame speed, provided that diffusive fluxes through the inlet of the flow domain are negligible [6].

Laminar flame thickness. In the case of diffusion-limited flame propagation with negligible chemical reaction upstream of and within the preheat layer, the thermal thickness of the flame front l_f scales with the thermal diffusivity α and laminar flame speed as [21]

$$l_f \sim \frac{\alpha}{s_f}. \tag{1}$$

The thermal thickness is $l_f = \Delta T/(dT/dx)_{max}$, where ΔT is the temperature rise across the front and $(dT/dx)_{max}$ is the maximum thermal gradient within the flame. Since the variation of thermal diffusivity and flame speed with reactant properties are typically well-modelled by established empirical relations [e.g. 17], this scaling relationship provides a simple means for estimating how the reaction front thickness varies across a range of combustion conditions for which the flame front behaviour is deflagarative. This scaling relationship breaks down as the flame transitions into an ignition front. The transport equation for progress variable c within a stationary ignition front is

$$u\frac{\partial c}{\partial x} = \frac{\omega_c}{\rho}, \tag{2}$$

where x and u are the displacement and velocity normal to the flame and ω_c is the reaction source term for progress variable. The thermal thickness of the reaction front can be approximated using the progress variable gradient: $l_f \sim (\partial c/\partial x)^{-1}_{max}$, giving the relationship

$$l_f \sim \frac{\rho_u}{\omega_{c,max}} s_f, \tag{3}$$

in which the factor $\rho_u/\omega_{c,max}$ is positive, with magnitude dependent on the thermochemical state of the reactants. The relationship between l_f and s_f

therefore provides an indication of whether a flame front is *deflagarative* ($\sim$ Eq. 1) or *ignitive* ($\sim$ Eq. 3).

The objectives of this study are to investigate and to model the effects of different methane/n-heptane fuel blends and their pre-ignition chemistry on the speed of reaction fronts under dual-fuel compression-ignition engine conditions. The following section sets out the physical modelling and numerical approach adopted. The results are then analysed in order (1) to assess the effects on flame speed and structure due to thermal and chemical contributions of the different fuels; and (2) to develop a new modelling approach for reaction front speeds under autoignitive conditions.

2. Methodology

Simulations of adiabatic un-stretched one-dimensional laminar flames are used to investigate the combined effects of methane/n-heptane ratios and pre-ignition chemistry at engine-relevant temperatures. The effect of the pre-ignition chemistry is assessed by varying the residence time upstream of the flame front. The residence time τ_f at the flame front is evaluated as

$$\tau_f = \int_{x_i}^{x_f} \frac{1}{u(x)} dx, \tag{4}$$

where x_i is the $x-$location of the inlet to the solution domain, x_f is the location of the upstream edge of the flame, here defined as being half of one thermal thickness upstream of the maximum temperature gradient location.

Reactant mixtures are described in terms of their total-equivalence ratio, ϕ_{tot}, evaluated in the conventional manner by considering the stoichiometric oxygen-fuel ratio for the fuel mixture, and fuel-equivalence ratios. The fuel equivalence ratios are defined by $\phi_{CH_4} = \nu_{CH_4} Y_{(CH_4,u)}/Y_{(O_2,u)}$ and $\phi_{C_7H_{16}} = \nu_{C_7H_{16}} Y_{(C_7H_{16},u)}/Y_{(O_2,u)}$, where subscript u denotes the unburnt composition and ν_i is the stoichiometric oxygen-to-fuel mass ratio for the i^{th} fuel species. These definitions of the fuel equivalence ratio can be added to obtain the total equivalence ratio, $\phi_{tot} = \phi_{CH_4} + \phi_{C_7H_{16}}$.

The flames are simulated using the COSILAB one-dimensional flame solver [22] with multi-component molecular transport and semi-perfect gas models based on seven-coefficient polynomials for the temperature-dependence of thermodynamic properties. The methane/n-heptane chemistry is modelled using a 106 species mechanism for n-heptane combustion [23]. There are few experimental data available for autoignition and flame propagation in methane/n-heptane fuel blends. Therefore the chemical model has been selected on the basis of satisfactory autoignition and flame propagation predictions of experimental data for pure methane–air and n-heptane–air mixtures, and satisfactory agreement with more detailed models for autoignition and flame propagation in methane/n-heptane fuel blends. Validation data for the 106 species mechanism used are provided as supplementary material.

The COSILAB software employs adaptive grid refinement and a stationary flame solution is obtained using a modified-Newton method [22]. The grid-independence of the solution data presented in this paper has been established by incrementally tightening the adaptive grid error tolerances until numerical convergence is achieved, requiring between one and four hundred grid points, depending on the simulation conditions.

3. Results and Discussion

3.1. Effects of pre-ignition chemistry on flame speed

Figure 1 shows the variation of flame speed with residence time for pure methane, pure n-heptane and two methane/n-heptane fuel blends at 40 bar and 850 or 1000 K. The flame speed of the methane–air mixture remains approximately constant until the residence time approaches the ignition delay time, when it increases indefinitely, as observed previously by Habisreuther *et al.* [8]. For an unburned temperature of 1000 K where n-heptane–air mixtures exhibit single-stage ignition, the evolution of the flame speed of the n-heptane–air mixture is qualitatively similar to the pure methane case. However, for an unburned temperature of 850 K where n-heptane–air mixtures exhibit two-stage ignition,

the flame speed also increases in two distinct stages: the flame speed increases by 15 % when the residence time reaches the first-stage ignition delay time, then increases gradually during the second-stage ignition-delay, before increasing indefinitely as the residence time approaches final ignition delay time. The same two-stage increase in flame speed is observed for methane/n-heptane blends that show two-stage ignition behaviour, and the two-stage effect is stronger as the proportion of n-heptane increases.

Figure 2 shows that the first-stage increase in flame speed coincides with the first-stage increase in temperature, occurring between 0.13-0.18 ms residence time for 40 bar 850 K stoichiometric n-heptane–air flames. The flame speed is expected to be affected by the temperature increase, however consumption of major reactants and production of intermediate species by the pre-ignition chemical reactions ahead of the flame also affect flame speed. We conduct a numerical experiment in order to quantify the relative influence that the thermal and chemical changes have on the flame speed during first-stage ignition. The experiment isolates the effect of the intermediate species from the thermal effects by performing modified flame simulations in which we remove all intermediate species a short distance upstream of the flame while keeping the temperature unchanged following the procedure set out in the Appendix. Since the intermediate species have been removed from the modified flame, the change in the speed of the *Modified flame* shown in Fig. 2 is entirely due to the temperature rise and the consumption of major reactants ahead of the flame front. The results of the modified flame experiment indicate that that the first stage increase in flame speed is due to both thermal and chemical influences in approximately equal measure. Modelling for the flame speed should take each of these effects into account.

3.2. Effects of pre-ignition chemistry on flame thickness

Diffusion-limited (i.e. deflagarative) flame propagation is expected to exhibit a scaling relationship between flame thickness and flame speed given by Eq. 1. Figure 3 shows the variation of the high-temperature flame's speed with α/l_f

for premixed combustion of stoichiometric methane–air and n-heptane–air at a range of reactant temperature (T_u = 700 to 1000 K). Data are normalised by the short-residence time laminar flame speeds of methane ($s_{l,CH_4} = 0.79ms^{-1}$) and n-heptane ($s_{l,C_7H_16} = 1.20ms^{-1}$) at 850 K and 40 bar. Flames with short residence times (shown as circular symbols) follow the deflagarative scaling relationship as T_u is increased from 700 to 1000 K. The gradient of s_f with respect to α/l_f is greater for n-heptane–air flames due to the greater reactivity of n-heptane compared to methane. As residence time increases (dashed lines), the flame speed of the n-heptane–air mixture remains largely unchanged until the mixture undergoes first-stage ignition. Subsequently the reaction front speed increases, and the reaction front thickness initially reduces in accordance with the deflagarative scaling given in Eq. 1. Finally, as the temperature-based progress variable ($c \equiv (T - T_u)/(T_b - T_u)$) ahead of the flame reaches 0.15, the deflagarative scaling breaks down and the front thickness starts to increase (α/l_f reduces) as the residence time ahead of the flame approaches the ignition delay time – marking the transition from deflagarative to ignitive scaling of the front thickness.

Figure 4 presents the variation of the cool-flame's speed and thickness for the 850 K 40 bar stoichiometric n-heptane–air flame as the residence time increases. The thickness of the cool-flame follows the linear scaling behaviour given for ignition fronts in Eq. 3. Despite its name, the cool-flame exhibits ignitive rather than deflagarative behaviour across all of the conditions in this study. The absence of deflagarative cool-flames is consistent with Ref. [24], where steady deflagarative cool-flames could only be stabilised when aerodynamic straining was used to prevent the development of a high-temperature flame. These observations support a hypothesis that deflagarative cool-flames, if they arise, do not survive in premixed combustion configurations in which the cool-flame is chased by a high-temperature flame – since the high-temperature flame speed would typically be fast enough to overtake a diffusion-limited cool-flame.

The transition between deflagarative and ignitive scaling of the flame thickness is accompanied by diminishing importance of diffusive transport within the

flame fronts. Figure 5 shows mass fraction transport budgets for stoichiometric n-heptane flames at 850 K and 40 bar for two residence times $\tau_f/\tau_{ign} = 0.85$ and 0.95. The reaction (R), convection (C) and diffusion (D) terms [6] are presented for the alkyl hydroperoxy radical (QOOH) within the cool-flame and for OH within the high-temperature flame front. The budgets indicate that diffusive transport in the high-temperature reaction front becomes gradually less important as the residence time increases, and is generally less important in the cool-flame front. The magnitude of the diffusion term in the high-temperature flame is lower at $\tau_f/\tau_{ign} = 0.95$, at which point the flame thickness is increasing with flame speed, than at $\tau_f/\tau_{ign} = 0.85$, at which point the flame thickness is reducing in accordance with the deflagarative scaling (Eq. 1). However the gradual reduction of the diffusive transport contribution does not provide as clear a delineation of the transition between deflagarative and ignitive behaviours as the changes in the $s_f - l_f$ dependence shown in Figs. 3 and 4.

Analysis of the flame thickness indicates that the deflagarative scaling in Eq. 1 applies to the high-temperature flame front across a wide range of autoignitive conditions and, given models for s_f and α, provides a useful means of modelling the variation of l_f in a flow. Eq. 1 is not applicable to cool-flames or to high-temperature flames burning through mixture that exhibits ignitive behaviour, however this restriction is not very limiting since the flame thickness was sought for use in flamelet combustion models, and such models are not expected to be valid in relation to flames with ignitive behaviour.

3.3. Modelling methane/n-heptane flame speeds for dual-fuel engines.

The laminar flame speed is a key input for a number of turbulent combustion models [16]. Several empirically-derived algebraic models for laminar flame speed have been developed and used widely for combustion at non-autoignitive conditions [e.g. 17]. For applications involving flame propagation through inhomogeneous mixtures of natural-gas/diesel or methane/n-heptane, the preceding results suggest that it would be beneficial to employ a laminar flame speed model that accounts both for the local composition of the fuel blend, and for

the effects of pre-ignition chemistry. Algebraic modelling for these effects is developed following a three step approach. First, established empirical models for the variation of flame speed with temperature, pressure, equivalence ratio and dilution are calibrated for pure methane and for pure n-heptane fuels at engine-relevant conditions. Second, new modelling is introduced to account for the effects of pre-ignition chemistry on the flame speed – accounting for the distinct contributions of heat release, reactant consumption, and enhanced reactivity ahead of the flame. Third, a mixing rule is employed in order to model the flame speed in methane/n-heptane mixtures based on the flame speed of the pure fuels.

Step 1: Flame speeds of pure fuels. The laminar flame speeds for pure methane and pure n-heptane fuels are evaluated for a set of engine-relevant conditions, recording the converged flame speed in the limit where the flame residence time is much less than the ignition delay time. Algebraic functions describing the dependence of flame speed on equivalence ratio [25] and unburnt-temperature, pressure and dilution [17] are then fitted to this data. Simulation data for the variation of methane and n-heptane flame speeds with equivalence ratio at reference conditions of $T_{u,ref} = 850$ K and $p_{ref} = 40$ bar are presented in Fig. 6. The variation of flame speed with equivalence ratio at these conditions is adequately modelled by a four-parameter Gaussian function [25],

$$s_{l,ref} = A_1 \phi_{tot}^{-A_2} \exp\left[-A_3 (\phi_{tot}^{-A_4})^2\right]. \tag{5}$$

$\mathbf{A} = \{A_1, A_2, A_3, A_4\}$ is a set of fitted coefficients for a particular fuel. At $T_{u,ref} = 850$ K and $p_{ref} = 40$ bar, we obtain $\mathbf{A}_{CH_4} = \{11500, -5.44, 1.20, -1.04\}$ and $\mathbf{A}_{C_7H_{16}} = \{344000, -4.80, 0.628, -2.56\}$ by least-squares fitting across the range $0.45 < \phi_{tot} < 1.3$, yielding the close agreement shown in Fig. 6.

Metghalchi and Keck [17] provide the following empirical model for the dependence of flame speed on the unburnt temperature T_u, pressure p, equivalence ratio ϕ_{tot} and the mass fraction ξ of diluents such as recirculated combustion

products,

$$s_{l,fuel} = s_{l,ref}(\phi_{tot}) \cdot \left(\frac{T_u}{T_{u,ref}}\right)^{\alpha} \cdot \left(\frac{p}{p_{ref}}\right)^{\beta} \cdot \gamma. \quad (6)$$

α, β and γ are model parameters given by expressions of the form: $\alpha = B_1 - B_2(\phi_{tot} - 1)$; $\beta = -B_3 + B_4(\phi_{tot} - 1)$; $\gamma = 1 - B_5\xi$, in which $\mathbf{B}_{fuel} = \{B_1, B_2, B_3, B_4, B_5\}$ is a set of fitted constants. Metghalchi and Keck fitted $\mathbf{B}_{fuel}$ values using flame speed data for unburnt temperatures up to 700 K, however these values are not generally applicable to flames at the higher-temperatures found in piston engines. We obtain $\mathbf{B}_{CH_4} = \{3.04, 0.70, 0.40, 0.10, 2.49\}$ and $\mathbf{B}_{C_7H_{16}} = \{2.79, -0.05, 0.26, 0.02, 3.02\}$ by least-squares fitting to a set of 45 flame speeds for each fuel at conditions comprising $T_u = \{700, 775, 850, 925, 1000\}$ K, $p = \{20, 40, 60\}$ bar, and $\phi_{tot} = \{0.8, 1, 1.2\}$. In order to evaluate B_5, four additional diluted flames are included with $\xi = \{0.00, 0.05, 0.10, 0.15\}$ at $\phi_{tot} = 1.0$, $T_u = 850$ K and $p = 40$ bar. The rms error of the fits for $\mathbf{B}_{CH_4}$ and $\mathbf{B}_{C_7H_{16}}$ are $0.020ms^{-1}$ and $0.028ms^{-1}$, and the maximum relative error of 10% occurs at the coldest and leanest conditions. The dataset used for parameter fitting is provided as supplementary material.

Step 2: Flame speeds at autoignitive conditions. Figure 7 shows that the laminar flame speed at autoignitive conditions increases approximately linearly with the value of progress variable just ahead of the flame for the full range of methane/n-heptane fuel blends investigated. Therefore modelling for the flame speed at autoignitive conditions will be developed as a function of the progress variable in the form

$$s_{f,fuel} = s_{l,fuel}\,(1 + \zeta_{fuel} c) \quad (7)$$

where ζ_{fuel} is a model coefficient and progress variable is based on temperature. Figure 7 reports values for progress variable two thermal thicknesses ahead of the location of the peak temperature gradient in the flame, however results show low sensitivity to distances between one and five thermal thicknesses ahead of the flame. The data presented in Fig. 7 suggests that $\zeta_{fuel} \approx 2.4 \pm 0.5$ for the blends considered ($\phi_{CH_4}/\phi_{tot} = 0, 0.5, 0.8, 1.0$) for progress variable less than

0.1. Super-linear behaviour is expected as the residence time approaches the ignition delay and the flame transitions into an ignition front, however flamelet-based turbulent combustion models that require flame speed as an input would not be applicable to flames with ignitive, rather than deflagarative behaviour. Therefore the linear modelling approach remains valid for diffusion-limited combustion conditions at which the flamelet approach is applicable.

Since the variation of ζ among methane/n-heptane fuel blends is relatively small it is convenient to adopt a single value of ζ for the full range of fuel blends. Figure 1 shows that using $\zeta = 2.4$ in Eq. 7 provides an adequate prediction of the variation of flame speed with residence time for all of the fuel blends and temperatures investigated. In order to apply the flame speed model in engine simulations, the progress variable in the mixture ahead of the flame then needs to be modelled, either by simulating the evolution of the chemical composition during ignition as in Ref. [26], or potentially by modelling the progress variable as a function of the Livengood-Wu integral [27].

Analysis in Section 3.1 shows that the flame speed is affected by the accumulation of intermediate species ahead of the flame, in addition to the effects of heat release and dilution due to reactant consumption. Equation 6 contains factors accounting for effects of temperature and dilution of the *unburned mixture* on flame speed. Similar factors may be applied to account for effects of the increase of temperature and dilution of reactants due to pre-ignition reactions ahead of the flame front: $(T/T_u)^{\alpha}$ and $1 - B_5\xi_{pr}$, where ξ_{pr} is the fraction of the reactants that have been consumed by pre-ignition reactions. Additional modelling is then necessary to account for the increased reactivity due to the accumulation of intermediate species ahead of the flame.

The increase in flame speed due to the presence of intermediate species is shown for stoichiometric n-heptane–air at 850 K by the difference between s_f and $s_{f,mod}$ in Fig. 2. Fig. 7 shows that $s_f/s_{f,mod}$ also has an approximately linear dependence on progress variable given by $1+\delta_{C_7H_{16}}c$, with $\delta_{C_7H_{16}} \approx 1.18$. Finally, thermal expansion due to pre-ignition heat release changes the velocity of the flow into which the high-temperature flame propagates. Accounting for

the thermal expansion upstream of a one-dimensional planar flame, the flame speed is multiplied by the density ratio ρ/ρ_u where ρ is the fluid density just upstream of the flame, finally giving

$$s_{f,fuel} = s_{l,fuel} \cdot \left(\frac{T}{T_u}\right)^{\alpha_{fuel}} \cdot (1 - B_{5,fuel}\xi_{pr}) \cdot (1 + \delta_{fuel}c) \cdot \left(\frac{\rho}{\rho_u}\right). \quad (8)$$

Each of the factors in Eq. 8 can be expressed as a function of progress variable: rearranging the definition of progress variable gives $T/T_u = 1 + c(T_b/T_u - 1)$; approximating the fraction of reactants that have been consumed by the progress variable gives $\xi_{pr} \approx c$; and, neglecting changes in pressure and molar mass, the ideal gas equation gives $\rho/\rho_u \approx [1 + c(T_b/T_u - 1)]^{-1}$. Since the model is only required to be valid for small values of progress variable, a first-order Taylor expansion of Eq. 8 yields

$$s_{f,fuel} = s_{l,fuel}\left(1 + c\left[(\alpha_{fuel} - 1) \times \left(\frac{T_u}{T_b} - 1\right) - B_{5,fuel} + \delta_{fuel}\right]\right). \quad (9)$$

Entering the previous values for stoichiometric n-heptane fuel ($\alpha_{C_7H_{16}} = 2.79$, $T_u/T_b = 3.18$, $B_{5,C_7H_{16}} = 3.02$, $\delta_{C_7H_{16}} = 1.18$) in Eq. 8 corresponds to a value of $\zeta_{C_7H_{16}} = 2.1$ in Eq. 7, which is reasonably close to the value of $\zeta \approx 2.4$ obtained from Fig. 7. Equations 8 and 9 therefore provide a breakdown of the various contributions to the flame speed increase.

Step 3: Flame speeds of mixtures. In order to model the laminar flame speed $s_{f,mix}$ in methane/n-heptane blends we compare the linear [25], Hirasawa *et al.* [28], and Di Sarli *et al.* [29] mixing-rules in Fig. 6. The Di Sarli *et al.* model tends to over-emphasise the contribution of methane. The linear model is simpler and marginally more accurate than the Hirasawa *et al.* model for methane/n-heptane blends, and it is adopted hereafter although either model is acceptable. The linear model is given by

$$s_{f,mix} = Z_{CH_4} s_{f,CH_4} + (1 - Z_{CH_4}) s_{f,C_7H_{16}}, \quad (10)$$

where $Z_{CH_4} = Y_{CH_4,u}/(Y_{CH_4,u} + Y_{C_7H_{16},u})$ is the local mass fraction of methane in the fuel blend. In agreement with Bourque *et al.* [30], adding higher-hydrocarbons to methane increases the flame speed disproportionately under

fuel-rich conditions. Potentially, a dependence on equivalence ratio could be incorporated into Eq. 10 in order to achieve even closer agreement. The complete new model is validated for a range of stoichiometric methane/n-heptane fuel blends in Fig. 1 and for the full range of lean equivalence ratios in Fig. 6 (solid circles), adequately capturing the effects of pre-ignition chemistry on flame speed across the full range of conditions with deflagarative behaviour.

4. Conclusions

The effects of pre-ignition chemistry on laminar flame speed in autoignitive methane/n-heptane fuel blends are investigated using premixed laminar flame simulations. The flame speed and thickness are important input parameters for turbulent combustion models based on flamelet assumptions.

Pre-ignition reactions cause the speed of the flame to increase. Fuels that exhibit two-stage ignition behaviour, such as n-heptane, also exhibit a two-stage increase in the speed of the reaction front as the reactant residence time increases. The increase in flame speed is due to distinct contributions of heat release, reactant consumption, and enhanced reactivity ahead of the flame. Addition of methane to n-heptane–air mixtures retards and reduces the first-stage increase in flame speed, in part due to dilution of the more-reactive n-heptane fuel, and in part due to consumption of radical species by the methane chemistry. As the residence time of the reactants approaches the ignition delay time, the reaction front transitions into a pure ignition front, in which diffusive transport is negligible.

Prior to transitioning into a pure ignition front, the behaviour of the flame can be classified as deflagarative or ignitive depending whether the flame thickness and flame speed obey the deflagarative scaling $l_f \sim \alpha/s_l$, subject to perturbations of the temperature ahead of the flame. The thickness of cool-flames exhibits ignitive scaling with flame speed, $l_f \sim s_f$, for all conditions simulated. The transition between deflagarative and ignitive scaling for high-temperature flame fronts occurs in 850 K stoichiometric n-heptane–air at a mixture residence

time of around 93% of the ignition delay time, as the progress variable in mixture ahead of the flame passes 0.15. The transition between deflagarative and ignitive scaling is associated with a reduction in the relative magnitude of diffusive transport within the flame front, however examination of the transport budget alone does not provide a clear delineation between deflagarative and ignitive behaviours.

Modelling for flame speed in dual-fuel blends at autoignitive conditions should account for the local composition of the fuel blend, and for the effects of pre-ignition chemistry. A linear mixing rule is adequate to describe the variation of flame speed in methane/n-heptane fuel blends. Modelling is introduced to account for the effects of pre-ignition chemistry on the flame speed. The model is a simple linear function of the progress variable ahead of the flame – accounting for the distinct contributions of heat release, reactant consumption, and enhanced reactivity ahead of the flame. The flame speed model accurately describes the variation of flame speed and hence flame thickness for the full range of methane/n-heptane blends at engine-relevant conditions, up to the deflagaration/ignition transition.

Appendix

Procedure for removing intermediate species ahead of the flame. The modified flame simulation involves two steps illustrated in Fig. 8.

Step 1. The first step involves a single precursor flame simulation (Fig. 8 top) that is used to determine the variation of the reactant composition with residence time upstream of the flame front. The composition recorded for each residence time is then modified by replacing the intermediate species with a mixture of reactants and major products of stoichiometric combustion. The replacement mixture consists of CH_4, C_7H_{16}, O_2, N_2, CO_2, and H_2O. The modified mixture composition is determined as a function of the fuel equivalence ratios (ϕ_{C7H16} and ϕ_{CH4}), the temperature T_u of the original unburnt mixture, and the local temperature T recorded from the precursor flame. The modified mass fraction

vector $\mathbf{Y}'$ is calculated by weighting the unburnt and burnt composition, $\mathbf{Y}_u$ and $\mathbf{Y}_b$ respectively, with a progress variable c_Y

$$\mathbf{Y}' = \mathbf{Y}_b c_Y + \mathbf{Y}_u(1 - c_Y). \tag{11}$$

The burnt composition is taken as the products of complete stoichiometric combustion, consisting of N_2, CO_2 and H_2O. The progress variable c_Y is given by

$$c_Y = \frac{\sum_{\alpha=1}^{nspec} [Y_\alpha h_\alpha(T) - Y_{\alpha,u} h_\alpha(T_u)]}{\sum_{\alpha=1}^{nspec} [Y_{\alpha,b} h_\alpha(T_b) - Y_{\alpha,u} h_\alpha(T_u)]}, \tag{12}$$

where $\mathbf{Y}$ and T are the original unmodified mass fraction vector and temperature, and h_α is the specific enthalpy of each species.

Step 2. The second step produces a flame solution using the modified composition as the inlet condition with the flame positioned 67μm from the inlet (Fig. 8 bottom). The flame residence time for the modified flame simulation is sufficiently small that the results are not influenced significantly by chemical reaction upstream of the modified flame front, and sufficiently large that the flame speed is not influenced significantly by diffusive flux through the domain inlet. This is confirmed in Fig. 2 by applying the two-step procedure without removing intermediate species from the reactant mixture: the flame speeds obtained using this 'reduced' solution domain closely follow the residence time-dependence obtained using a single 'full' solution domain. The difference due to the use of the reduced domain procedure is negligible compared with the effect of replacing the intermediate species. This confirms the validity of the modified flame approach for determining the relative influences of intermediate species and thermal effects.

Declaration of interest

The authors are thankful for financial support from CNPq (Brazil) grant 207250/2014-6 and EPSRC (UK) grant EP/K024876/1.

Data statement

All data supporting this study are openly available from the University of Southampton repository at (doi to be provided upon acceptance).

References

[1] B. Windom, S. H. Won, C. B. Reuter, B. Jiang, Y. Ju, S. Hammack, T. Ombrello, C. Carter, Study of ignition chemistry on turbulent premixed flames of n-heptane/air by using a reactor assisted turbulent slot burner, Combustion and Flame 169 (2016) 19 – 29. doi:https://doi.org/10.1016/j.combustflame.2016.02.031.

[2] G. A. Lavoie, J. Martz, M. Wooldridge, D. Assanis, A multi-mode combustion diagram for spark assisted compression ignition, Combustion and Flame 157 (6) (2010) 1106 – 1110. doi:https://doi.org/10.1016/j.combustflame.2010.02.009.

[3] S. H. Won, B. Windom, B. Jiang, Y. Ju, The role of low temperature fuel chemistry on turbulent flame propagation, Combustion and Flame 161 (2) (2014) 475 – 483. doi:https://doi.org/10.1016/j.combustflame.2013.08.027.

[4] Z. Wang, Y. Qi, X. He, J. Wang, S. Shuai, C. K. Law, Analysis of pre-ignition to super-knock: Hotspot-induced deflagration to detonation, Fuel 144 (2015) 222 – 227. doi:https://doi.org/10.1016/j.fuel.2014.12.061.

[5] F. L. Dryer, Chemical kinetic and combustion characteristics of transportation fuels, Proceedings of the Combustion Institute 35 (1) (2015) 117 – 144. doi:https://doi.org/10.1016/j.proci.2014.09.008.

[6] A. Krisman, E. R. Hawkes, J. H. Chen, The structure and propagation of laminar flames under autoignitive conditions, Combustion and Flame

188 (2018) 399 – 411. doi:https://doi.org/10.1016/j.combustflame.2017.09.012.

[7] T. Korakianitis, A. M. Namasivayam, R. J. Crookes, Natural-gas fueled spark-ignition (SI) and compression-ignition (CI) engine performance and emissions, Progress in Energy and Combustion Science 37 (1) (2011) 89–112.

[8] P. Habisreuther, F. C. C. Galeazzo, C. Prathap, N. Zarzalis, Structure of laminar premixed flames of methane near the auto-ignition limit, Combustion and Flame 160 (12) (2013) 2770 – 2782. doi:https://doi.org/10.1016/j.combustflame.2013.06.023.

[9] F. Battin-Leclerc, Detailed chemical kinetic models for the low-temperature combustion of hydrocarbons with application to gasoline and diesel fuel surrogates, Progress in Energy and Combustion Science 34 (4) (2008) 440 – 498. doi:https://doi.org/10.1016/j.pecs.2007.10.002.

[10] J. F. Griffiths, S. K. Scott, Thermokinetic interactions: Fundamentals of spontaneous ignition and cool flames, Progress in Energy and Combustion Science 13 (3) (1987) 161 – 197. doi:https://doi.org/10.1016/0360-1285(87)90010-4.

[11] H. K. Ciezki, G. Adomeit, Shock-tube investigation of self-ignition of n-heptane-air mixtures under engine relevant conditions, Combustion and Flame 93 (4) (1993) 421 – 433. doi:https://doi.org/10.1016/0010-2180(93)90142-P.

[12] J. Pan, H. Wei, G. Shu, Z. Chen, P. Zhao, The role of low temperature chemistry in combustion mode development under elevated pressures, Combustion and Flame 174 (2016) 179 – 193. doi:https://doi.org/10.1016/j.combustflame.2016.09.012.

[13] S. K. Aggarwal, O. Awomolo, K. Akber, Ignition characteristics of heptane–

hydrogen and heptane–methane fuel blends at elevated pressures, international journal of hydrogen energy 36 (23) (2011) 15392–15402.

[14] S. Schlatter, B. Schneider, Y. Wright, K. Boulouchos, Experimental study of ignition and combustion characteristics of a diesel pilot spray in a lean premixed methane/air charge using a rapid compression expansion machine, Tech. rep., SAE Technical Paper (2012).

[15] E. Demosthenous, G. Borghesi, E. Mastorakos, R. S. Cant, Direct numerical simulations of premixed methane flame initiation by pilot n-heptane spray autoignition, Combustion and Flame 163 (2016) 122–137.

[16] N. Peters, Turbulent Combustion, Cambridge Monographs on Mechanics, Cambridge University Press, 2000. doi:10.1017/CBO9780511612701.

[17] M. Metghalchi, J. C. Keck, Burning velocities of mixtures of air with methanol, isooctane, and indolene at high pressure and temperature, Combustion and flame 48 (1982) 191–210.

[18] D. Shin, R. D. Sandberg, E. S. Richardson, Self-similarity of fluid residence time statistics in a turbulent round jet, Journal of Fluid Mechanics 823 (2017) 1–25.

[19] Y. B. Zeldovich, Regime classification of an exothermic reaction with nonuniform initial conditions, Combustion and Flame 39 (2) (1980) 211 – 214. doi:https://doi.org/10.1016/0010-2180(80)90017-6.

[20] F. A. Williams, The mathematics of combustion, SIAM, Philadelphia 97.

[21] S. R. Turns, An introduction to combustion, 2000, MacGraw Hill, Boston, Massachusetts, US.

[22] Cosilab software, Tech. rep., Cosilab, Rotexo Software, Bochum (2011).

[23] E. Ranzi, A. Frassoldati, A. Stagni, M. Pelucchi, A. Cuoci, T. Faravelli, Reduced kinetic schemes of complex reaction systems: fossil and biomass-

derived transportation fuels, International Journal of Chemical Kinetics 46 (9) (2014) 512–542.

[24] P. Zhao, W. Liang, S. Deng, C. K. Law, Initiation and propagation of laminar premixed cool flames, Fuel 166 (2016) 477 – 487. doi:https://doi.org/10.1016/j.fuel.2015.11.025.

[25] S. Yang, R. D. Reitz, Integration of a continuous multi-component fuel evaporation model with an improved g-equation combustion and detailed chemical kinetics model with application to gdi engines, Tech. rep., SAE Technical Paper (2009).

[26] B. S. Soriano, E. S. Richardson, S. Schlatter, Y. M. Wright, Conditional moment closure modelling for dual-fuel combustion engines with pilot-assisted compression ignition, Tech. rep., SAE Technical Paper (2017).

[27] J. C. Livengood, P. C. Wu, Correlation of autoignition phenomena in internal combustion engines and rapid compression machines, in: Symposium (international) on combustion, Vol. 5, 1955, pp. 347–356.

[28] T. Hirasawa, C. J. Sung, A. Joshi, Z. Yang, H. Wang, C. K. Law, Determination of laminar flame speeds using digital particle image velocimetry: binary fuel blends of ethylene, n-butane, and toluene, Proceedings of the Combustion Institute 29 (2) (2002) 1427–1434.

[29] V. Di Sarli, A. Di Benedetto, Laminar burning velocity of hydrogen–methane/air premixed flames, International Journal of Hydrogen Energy 32 (5) (2007) 637–646.

[30] D. Healy, N. S. Donato, C. J. Aul, E. L. Petersen, C. M. Zinner, G. Bourque, H. J. Curran, n-butane: Ignition delay measurements at high pressure and detailed chemical kinetic simulations, Combustion and Flame 157 (8) (2010) 1526–1539.

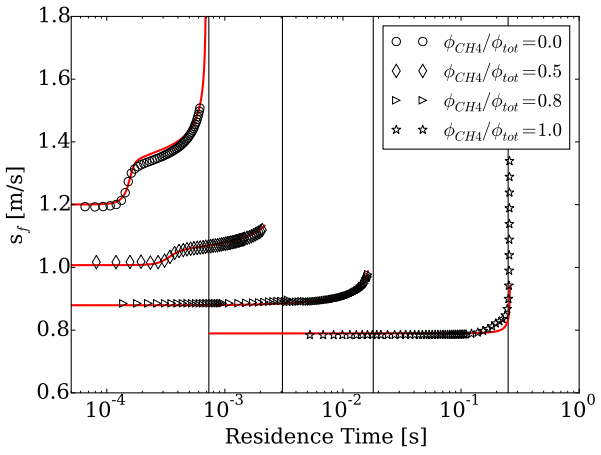

(a) 850 K

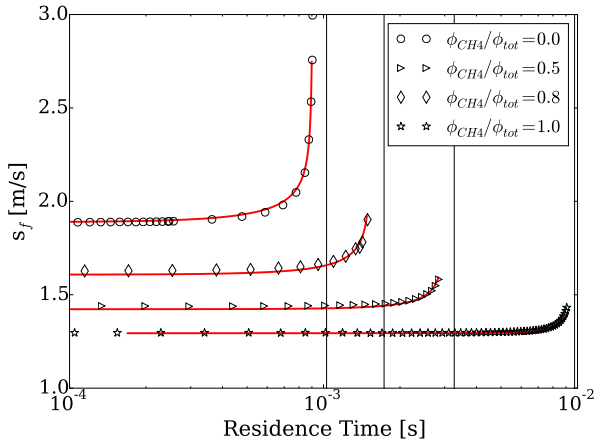

(b) 1000 K

Figure 1: Laminar flame speeds of stoichiometric methane/n-heptane blends versus residence time at 40 bar: simulations (symbols); model Eqs. 7 and 10 (solid).

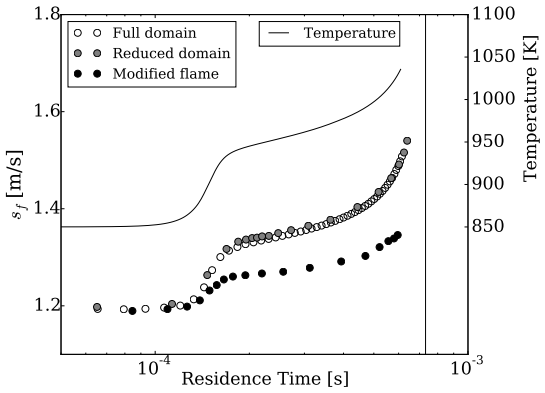

Figure 2: Laminar flame speed and temperature versus residence time for stoichiometric n-heptane–air at 40 bar and 850 K: Unmodified flame in the full domain (white circles); 0.2 mm domain with inlet composition from the unmodified flame (grey circles); 0.2 mm domain with intermediate species removed from the inlet composition (black circles).

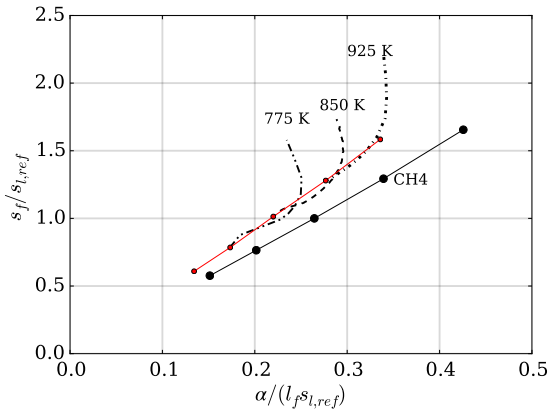

Figure 3: Normalised high-temperature reaction front speed $s_f/s_{l,ref}$ versus $\alpha/(l_f s_{l,ref})$ for short residence time stoichiometric methane–air and n-heptane–air flames with unburnt temperatures 700, 775, 850, 925 and 1000 K (symbols). Data for n-heptane–air combustion with residence times up to 98% of the ignition delay time at 775, 850, and 925 K (various dashed lines as labelled).

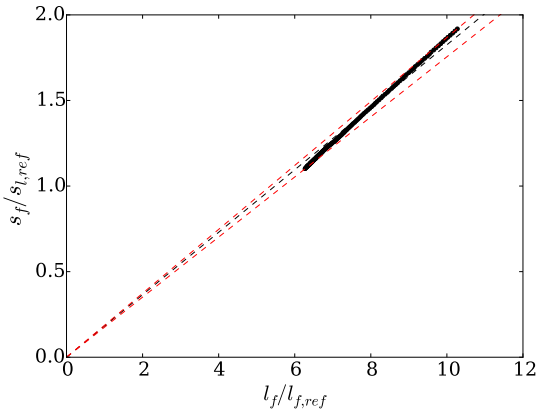

Figure 4: Cool-flame reaction front speed s_f versus thermal thickness l_f for stoichiometric n-heptane–air flames at 850 K and 40 bar for a range of residence times (symbols). Dashed lines correspond to Eq. 3.

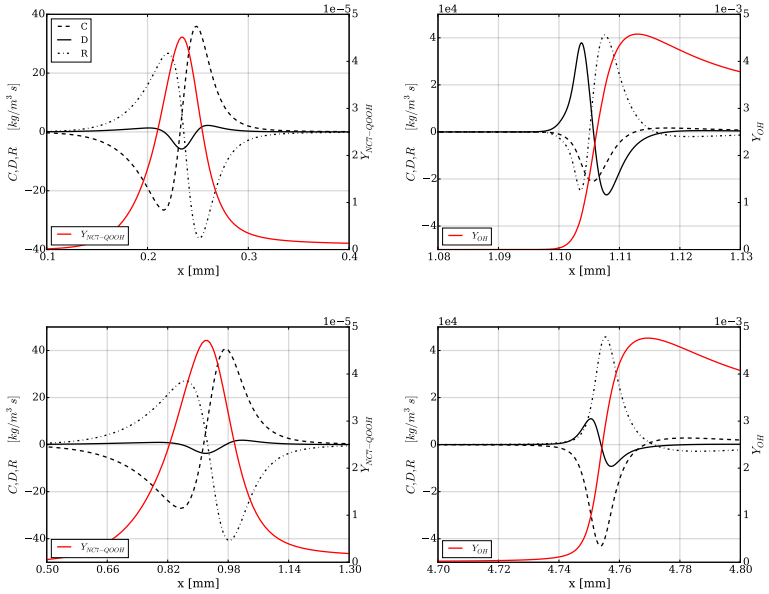

Figure 5: Transport budgets and mass fraction profiles for stoichiometric n-heptane–air at 850 K and 40 bar for Y_{QOOH} (left column) and Y_{OH} (right column). The residence times at the flame front are 85% (top row), and 95% (bottom row) of the overall ignition delay time. The data are plotted versus the distance from the inlet.

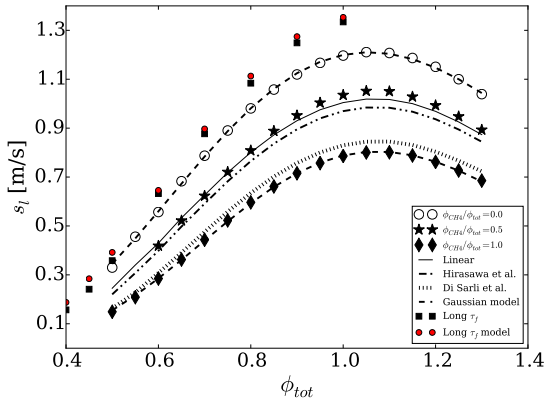

Figure 6: Variation of flame speed with equivalence ratio for methane/n-heptane fuel blends at 850 K and 40 bar for $\phi_{CH4}/\phi_{tot} = 0$, 0.5 and 1.0; Fitted flame speeds from Eq. 5; and linear [25], Hirasawa *et al.* [28], and Di Sarli *et al.* [29] mixing-rules. Speeds for a long residence time flame from simulations and from predictions of the model (Eqs. 7 and 10) are also shown.

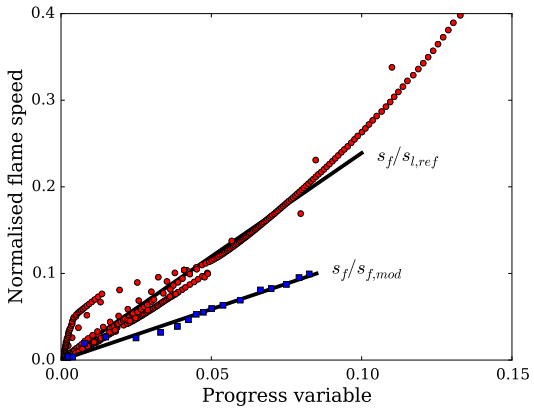

Figure 7: Normalised flame speed versus the progress variable upstream of the flame front: Round symbols show $s_f/s_{l,ref}$ at $\phi_{CH_4}/\phi_{tot} = 0$, 0.5, 0.8 and 1.0 for $T_u = 850$ K and 1000 K; Square symbols show $s_f/s_{f,mod}$ based on data from Fig. 2. Solid lines show $s_f/s_{l,ref} = 2.4c$ and $s_f/s_{f,mod} = 1.18c$.

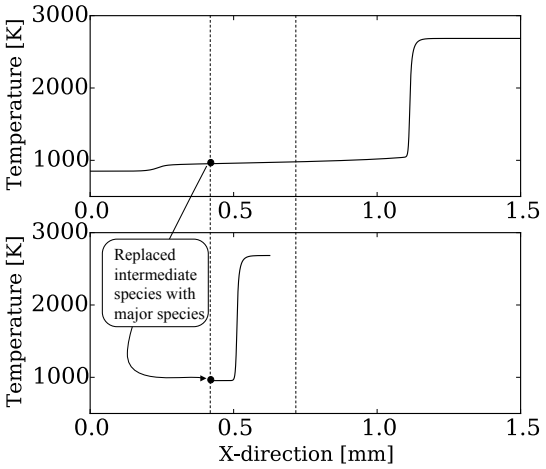

Figure 8: Illustration of the reduced-domain simulation procedure: temperature field from a full-domain simulation of a stoichiometric n-heptane–air flame with $\tau_f = 0.95\tau_{ign}$ (top); temperature field from the reduced-domain simulation.